Amplitude modulated flow analysis for speciation—Proof of concept by quantification of Fe^{2+} and Fe^{3+} ions

Hideji Tanaka [a,b,*], Yohei Kurokawa [b], Masaki Takeuchi [a,b], Akira Ohbuchi [c]

[a] *Institute of Biomedical Sciences, Tokushima University, 1-78-1 Shomachi, Tokushima 770-8505, Japan*
[b] *Graduate School of Pharmaceutical Sciences, Tokushima University, 1-78-1 Shomachi, Tokushima 770-8505, Japan*
[c] *Graduate School of Technology, Industrial and Social Sciences, Tokushima University, 2-1 Minami-Josanjima, Tokushima 770-8506, Japan*

ARTICLE INFO

ABSTRACT

We propose a novel concept of flow-based analysis for spectrophotometric speciation based on flow rate modulation and fast Fourier transform (FFT). A redox reagent solution's and a sample solution's flow rates are varied by sinusoidal control signals with periods of T and $0.5T$, respectively. Both solutions are merged with a color reagent, while the total flow rate is held constant. Downstream, the absorbance of the mixed solution is measured and acquired as the detector output voltage (V_d). The V_d is analyzed by FFT with the window's time length of T. One species that directly reacts with the color reagent contributes only to the amplitude (A_2) of the second harmonic wave component in V_d. The other species that needs the redox conversion before the coloration contributes to the amplitude (A_1) of the fundamental wave component, in addition to A_2. The former species+' concentration can be estimated from A_2 by taking the latter's contribution to A_2 into account. The latter species' concentration can be determined only from A_1. The proposed concept was demonstrated by applying it to the speciation of Fe^{2+} and Fe^{3+} by an o-phenanthroline spectrophotometry, where Fe^{3+} was reduced to Fe^{2+} by L-ascorbic acid before the coloration.

1. Introduction

Amplitude-modulated multiplexed flow analysis (AMMFA), first proposed in 2008 by Tanaka et al. [1], is a flow-based analysis with flow rate modulation and frequency analysis. The pieces of information on analytes in multiple sample solutions are amplitude-modulated by varying their flow rates at different frequencies. The merged solution's analytical signal is measured downstream and analyzed by fast Fourier transform (FFT). The concentrations of the analytes in the samples are simultaneously determined from the corresponding wave component's amplitudes. We applied the concept to the simultaneous analysis of multiple samples [1,2]. A lock-in detection instead of FFT was also employed for the frequency analysis [3]. As variants of AMMFA, air-segmented AMMFA [4–6] and internal standard AMMFA [7] were also developed to improve the measurements' sensitivity and robustness, respectively.

In a previous paper [8], the concept of AMMFA was extended to the speciation of NO_2^- and NO_3^- in a sample by a Griess spectrophotometry [9]. The sample solution was delivered from two channels, where the flow rates were modulated at respective frequencies. One of the channels had a cadmium-cupper column for reducing NO_3^- to NO_2^-. However, except for this on-line pretreatment, the basic principle was essentially the same as that for multiple sample analyses [1,2,4–7] mentioned above.

In the present paper, a novel AMMFA concept for speciation is proposed. Not only the sample flow rate, but also the pretreatment reagent flow rate is varied at a different frequency. Both solutions are merged with a color reagent solution. Downstream, the absorbance of the merged solution is measured and analyzed by FFT. The speciation is carried out from the amplitudes of wave components in the analytical signal by considering the respective species' contributions to the individual amplitudes. As proof of the concept, it is applied to the speciation of Fe^{2+} and Fe^{3+} by an o-phenanthroline (o-Phen) spectrophotometry. L-ascorbic acid is used for reducing Fe^{3+} to Fe^{2+} before the coloration.

Various flow-based speciation based on redox chemical conversions have been reported, as reviewed by Trojanovics [10]. More recently, flow-based speciation of Sb(III)/Sb(V) [11], Cr(III)/Cr(VI) [12–14], NO_2^-/NO_3^- [15], V(IV)/V(V) [16], and As(III)/As(V) [17], for examples, were reported.

As for the speciation of iron, the approaches would be classified into two categories. The one is multi-detection methods, where Fe^{2+} and Fe^{3+} ions are independently sensed by respective sensing devices [18,19]. The other is quasi-simultaneous detection methods, where one of the ions and total ions are sequentially sensed with a single detector.
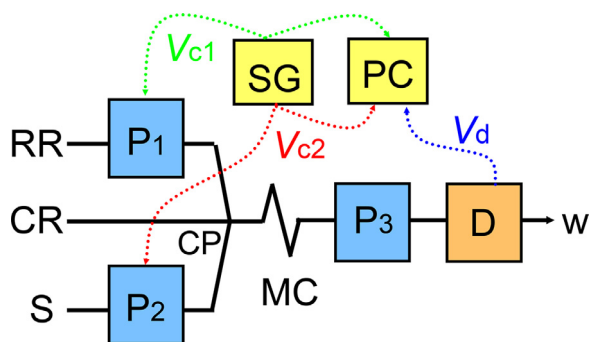
Fig. 1. Flow system. S, sample solution; RR, redox reagent solution; CR, color reagent solution; w, waste; P_1, P_2 and P_3, peristaltic pumps; MC, mixing coil; CP, confluence point; D, detector; SG, signal generator; PC, computer with A/D-D/A converter; V_{c1} and V_{c2}, control voltages; V_d, detector output voltage.

The latter includes merging zone FIA [20,21], double injection methods [22,23], circulating flow method [24], SIA [25,26], multi-pumping flow analysis [27], and Lab-in-syringe method [28]. Saavedra et al. [29] sequentially determined the ions by an amperometric FIA at different electrode potentials. Kozak et al. [30–32] determined the ions based on the change in their colored complex's absorbance in the presence or absence of EDTA. Mesquita, Rangel, et al. studied 3-hydroxy-4-pyridinone (3,4-HPO) chelators [33,34] as non-toxic colorimetric reagents for iron. They applied a hexadentate 3,4-HPO chelator to the speciation of iron by SIA with in-line solid phase extraction and realized the LOD as low as sub-0.1 μmol dm^{-3} level with a liquid waveguide capillary cell [34].

As for FFT application to flow analyses, Dyke and Fernando [35] reported a deconvolution technique coupled with FIA. The concept was demonstrated by using $KMnO_4$ as a sample. Szostek and Trojanowicz [36] reported an FIA with fast multiple injections of the same solution in a given constant time interval. The detector signals in the time domain were converted to those in the frequency domain. The NO_2^- concentration could be obtained from the amplitude of the wave component that has the period equaled to the injection time interval.

The concept proposed in the present study is entirely different from the preceding approaches described above because it is based on the modulation of flow rates of multiple liquid flows and the FFT analysis of the analytical signal.

2. Principle

Figs. 1 and 2A show the flow system configuration and the control signal profile that realize the proposed principle for speciation. The flow system is of a three-channel manifold, where redox reagent (RR), color reagent (CR), and sample (S) are delivered Fig. 1. The flow rates of RR and S are varied using P_1 and P_2 pumps that are controlled by the output voltages (V_{c1} and V_{c2}, respectively) from a signal generator (SG). The V_{c1} for controlling the RR flow rate is varied in the range from $-V_M$ to V_M with a period of T; V_{c2} for controlling the S flow rate is varied from 0 to $0.5V_M$ with a period of $0.5T$ (Fig. 2A). These control voltages are expressed by Eqs. (1) and (2), respectively, where t is time.

$$V_{c1}(t) = V_M \cos \frac{2\pi t}{T} \tag{1}$$

$$V_{c2}(t) = 0.25V_M \cos \frac{4\pi t}{T} + 0.25V_M \tag{2}$$

Both the solutions are merged with CR aspirated to the confluence point (CP) while the total flow rate is held constant with the P_3 pump. The CR concentration is set to be in excess over the analyte at any flow ratio of S and CR. Downstream, the absorbance of the merged solution is monitored with a UV/Vis detector (D). The output voltage V_d from D, as well as V_{c1} and V_{c2}, is acquired in a computer (PC) as digital data.
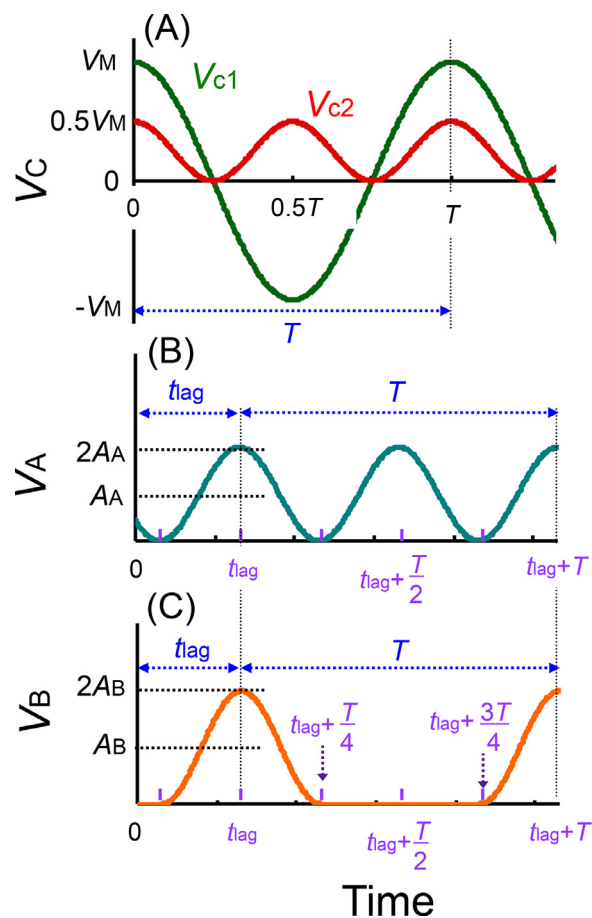

Fig. 2. Schematic signal diagrams for realizing the present principle. (A) Profile of control signals of V_{c1} (period: T, amplitude: V_M) and V_{c2} (period: $0.5T$, amplitude: $0.25V_M$; offset: $0.25 V_M$). (B) Profile of analytical signal (amplitude: A_A) caused by the species A, which directly reacts with a color reagent. (C) Profile of analytical signal (amplitude: A_B) caused by the species B, which needs to be converted to the species A before the coloration). T, the time length of FFT window (= the least common multiple of V_{c1} and V_{c2} periods); t_{lag}, lag time between mixing of solution upstream and it's being sensed downstream.

Analytical signal V_d is of periodic nature that has a period equals the least common multiple (i.e., T) of the V_{c1} and V_{c2} periods (T and $0.5T$, respectively). This T is set as the time length of the FFT window because the length should be an integral multiple of the period of analytical signal for discrete Fourier transform. The FFT computation is carried out according to the formula expressed as Eq. 3.

$$X_k = \frac{1}{N} \sum_{n=0}^{N-1} x_n \exp\left(-j\frac{2\pi nk}{N}\right)$$
$$= \frac{1}{N} \sum_{n=0}^{N-1} x_n \cos\frac{2\pi nk}{N} - j\frac{1}{N} \sum_{n=0}^{N-1} x_n \sin\frac{2\pi nk}{N}, \tag{3}$$

where N is the number of data for the FFT computation, and j is the imaginary number. X_0 corresponds to the direct current component in V_d; $2|X_1|$, $2|X_2|...2|X_{(N/2-1)}|$, and $|X_{N/2}|$ correspond to the amplitudes of the fundamental wave component, the second harmonic wave component ...the $(N/2 - 1)^{th}$ harmonic wave component, and the $(N/2)^{th}$ harmonic wave component, respectively. The FFT computation is carried out in real-time with a new N data set at regular intervals.

It is assumed that the species A reacts directly with CR, and the species B needs to be converted to A by RR before the coloration. The obtained V_d consists of the contributions from both A and B (Eq. (4)).

$$V_d = V_A + V_B, \tag{4}$$

where, V_A and V_B mean respective contributions to V_d. The V_A profile is expressed by Eq. (5) and schematically shown in Fig. 2B.

$$V_A(t) = A_A \cos\left\{\frac{4\pi}{T}\left(t - t_{lag}\right)\right\} + A_A, \tag{5}$$

where A_A is the amplitude. The A's coloration is independent of the RR flow rate. Therefore, the species A contributes only to the second harmonic wave component (period: $0.5T$) in V_d. The V_A profile Fig. 2B) is similar in shape to the V_{c2} profile (Fig. 2A) that controls the sample flow rate, but has a phase delay. This delay is attributed to the lag time (t_{lag}) between the merging of solutions upstream and the sensing of the corresponding signal downstream. In the present configuration, t_{lag} can be regarded as constant because the transit time from the merging point to the sensing point (CP and D in Fig. 1, respectively) is invariable under the constant total flow rate. On the other hand, the V_B profile would be expressed by Eqs. (6) and (7), as shown in Fig. 2C.

For $(n - 0.25)T + t_{lag} \leq t \leq (n + 0.25)T + t_{lag}$

$$V_B(t) = A_B \cos\left\{\frac{4\pi\left(t - t_{lag}\right)}{T}\right\} + A_B \tag{6}$$

For $(n + 0.25)T + t_{lag} < t < (n + 0.75)T + t_{lag}$

$$V_B(t) = 0, \tag{7}$$

where n and A_B mean an integer and the amplitude, respectively. When V_{c1} is negative, the species B cannot form the colored product because P_1 that feeds RR does not work. Therefore, there is a region where V_B is null in the profile (Eq. (7)). This results in the various wave components other than the second harmonic wave component in the V_B profile.

By applying the Fourier transform formulae, the Fourier coefficients of the cosine and sine terms ($a_{1,B}$ and $b_{1,B}$) for the fundamental wave component in the V_B profile can be obtained as expressed by Eqs. (8) and (9), respectively; for more detailed derivation processes, refer to *Derivation of Eq. (8)* and *Derivation of Eq. (9)* in the Supplementary Material.

$$
\begin{aligned}
a_{1,B} &= \frac{2}{T}\int_0^T V_B(t)\cos\frac{2\pi t}{T}\,dt \\
&= \frac{2}{T}\int_{t_{lag}}^{t_{lag}+\frac{T}{4}}\left\{A_B\cos\frac{4\pi\left(t - t_{lag}\right)}{T} + A_B\right\}\cos\frac{2\pi t}{T}\,dt \\
&\quad + \frac{2}{T}\int_{t_{lag}+\frac{3}{4}T}^{t_{lag}+T}\left\{A_B\cos\frac{4\pi\left(t - t_{lag}\right)}{T} + A_B\right\}\cos\frac{2\pi t}{T}\,dt \\
&= \frac{8A_B}{3\pi}\cos\frac{2\pi t_{lag}}{T}
\end{aligned}
\tag{8}
$$

$$
\begin{aligned}
b_{1,B} &= \frac{2}{T}\int_0^T V_B(t)\sin\frac{2\pi t}{T}\,dt \\
&= \frac{2}{T}\int_{t_{lag}}^{t_{lag}+\frac{T}{4}}\left\{A_B\cos\frac{4\pi\left(t - t_{lag}\right)}{T} + A_B\right\}\sin\frac{2\pi t}{T}\,dt \\
&\quad + \frac{2}{T}\int_{t_{lag}+\frac{3}{4}T}^{t_{lag}+T}\left\{A_B\cos\frac{4\pi\left(t - t_{lag}\right)}{T} + A_B\right\}\sin\frac{2\pi t}{T}\,dt \\
&= \frac{8A_B}{3\pi}\sin\frac{2\pi t_{lag}}{T}
\end{aligned}
\tag{9}
$$

Likewise, the Fourier coefficients of the cosine and sine terms ($a_{2,B}$ and $b_{2,B}$) for the second harmonic wave component are respectively expressed as follows.

$$a_{2,B} = \frac{2}{T}\int_0^T V_B(t)\cos\frac{4\pi t}{T}\,dt = \frac{A_B}{2}\cos\frac{4\pi t_{lag}}{T} \tag{10}$$

$$b_{2,B} = \frac{2}{T}\int_0^T V_B(t)\sin\frac{4\pi t}{T}\,dt = \frac{A_B}{2}\sin\frac{4\pi t_{lag}}{T} \tag{11}$$

More detailed derivation processes for Eqs. (10) and (11) are described in *Derivation of Eq. (10)* and *Derivation of Eq. (11)*, respectively, in the Supplementary Material. From Eqs. (8)–(11), the amplitudes of the fundamental and the second harmonic wave components of V_B are expressed by Eqs. (12) and (13), respectively.

$$A_{1,B} = \left(a_{1,B}{}^2 + b_{1,B}{}^2\right)^{1/2} = \frac{8A_B}{3\pi} \tag{12}$$

$$A_{2,B} = \left(a_{2,B}{}^2 + b_{2,B}{}^2\right)^{1/2} = \frac{A_B}{2} \tag{13}$$

It should be noted, however, Eqs. (12) and (13) can be derived more efficiently by considering the natures of periodic signal and discrete Fourier transform. That is, $V_B(t)$ is moved by t_{lag} in the negative direction of the abscissa and then integrated; details are also explained in *Derivation of Eqs. (12) and (13) after moving the $V_B(t)$ signal (Fig. 2C) by t_{lag} in the negative direction of the abscissa* in the Supplementary Material.

Therefore, $A_{2,B}$ can be expressed as a function of $A_{1,B}$ as follows,

$$A_{2,B} = \frac{\frac{A_B}{2}}{\frac{8A_B}{3\pi}}A_{1,B} = \frac{3\pi}{16}A_{1,B} \sim 0.5890A_{1,B} \tag{14}$$

Since the additive property is held in Fourier transform, the amplitudes of the fundamental and the second harmonic waves components (A_1 and A_2) in V_d are expressed by Eqs. (15) and (16), respectively, on the assumption that no coexisting species contribute to the analytical signal.

$$A_1 = A_{1,B} \tag{15}$$

$$
\begin{aligned}
A_2 &= A_{2,A} + A_{2,B} \\
&= A_{2,A} + \frac{3\pi}{16}A_1
\end{aligned}
\tag{16}
$$

The wave components' amplitudes are in proportion to the concentrations of the corresponding analytes [1]. Consequently, the B's concentration can be determined from A_1; the A's concentration can be estimated from A_2 by taking the B's contribution to A_2 (i.e., $\frac{3\pi}{16}A_{1,B}$) into account.

3. Experimental

3.1. Reagents

As a proof of the concept, we applied it to the speciation of Fe^{2+} (the species A) and Fe^{3+} (the species B) by an *o*-phenanthroline (*o*-Phen) spectrophotometry. All of the reagents used were of analytical reagent grade and were used without further purification. Sartorius Arium 611DI grade deionized water was used throughout. A 0.18 mol dm^{-3} acetate buffer (pH 4.6) was prepared by dissolving 3.2 g of acetic acid and 5.1 g of sodium acetate trihydrate, both of which were purchased from Nacalai Tesque (Kyoto, Japan), in water to make the final volume of 500 cm^3.

Ammonium iron(II) sulfate hexahydrate was purchased from Nacalai Tesque. A 1 mmol dm^{-3} Fe^{2+} solution was daily prepared by dissolving the salt with the acetate buffer. Ammonium iron(III) sulfate dodecahydrate was purchased from Wako Pure Chemical Industries (Osaka, Japan). A 1 mmol dm^{-3} Fe^{3+} solution was daily prepared by dissolving the salt with the acetate buffer. Respective 1 mmol dm^{-3} solutions were appropriately mixed and diluted with water to prepare solutions containing Fe^{2+} and Fe^{3+} in various concentrations. Thus prepared solutions were used as S (sample) in Fig. 1 in the experiments to validate the proposed concept.

L-ascorbic acid (AA), purchased from Kanto Chemicals (Tokyo, Japan), was dissolved in the acetate buffer to make a 0.15 mmol dm^{-3} solution. This solution was used as RR (redox reagent) in Fig. 1.

o-Phenanthroline (o-Phen) monohydrate, purchased from Kanto Chemicals, was dissolved in the acetate buffer to make a 10 mmol dm^{-3} solution. This solution was used as CR (color reagent) in Fig. 1.

3.2. Water samples

Real water samples were collected from the Yoshino River (rural area), the Sako River (urban area), and the Fuigo-onsen Spring in Tokushima Prefecture, Japan. Each sample was filtered through a disposable disk filter with a pore size of 0.45 μm (Kanto Chemicals, 96904–00, Tokyo, Japan) and stored in a polypropylene bottle at 4 ˚C.

3.3. Flow system

The flow system was constructed according to the configuration shown in Fig. 1. Polytetrafluoroethylene (PTFE) tubing (0.5 mm i.d.) was used as the conduit. The P_1-P_3 were Rainin Dynamax RP-1 peristaltic pumps (USA). Pharmed tubing with 0.51 mm i.d. was used for P_1 and P_2, and that with 0.79 mm i.d. was for P_3 as pump tubes. The flow rates of the AA solution and a sample solution were varied in the range from 0 to 1.1 cm^3 min^{-1} and 0 to 0.55 cm^3 min^{-1} by V_{c1} and V_{c2}, respectively, generated by a signal generator (SG; NF Co., WF1974, Japan). Both the solutions were merged with the o-Phen solution aspirated to the confluence point (polypropylene X-shaped Mini-Fitting. As One, VFX106, Japan) under the constant total flow rate of 2.5 cm^3 min^{-1}. The color reaction was accelerated in a mixing coil (MC; 1 m in length) immersed in a water bath. The residence time of the solution in MC was ca. 4.7 s. The temperature of the bath was maintained at 60 ˚C using a PID controller (TOP, TTM-64, Japan), a heater (TOP, SKH-0151, Japan), and a sensor (TOP, Pt-40–150, Japan). The occasionally generated bubbles were removed through a porous PTFE tubing (Sumitomo Fine Polymer, TB-0201, Japan) inserted downstream of P_3. The mixed solution was then led to a quartz flow cell (GL Sciences, 6001–70212, Japan; 9.6 mm optical path length, 8 mm^3 inner volume) set in a detector (D; GL Sciences, UV702 spectrophotometer, Japan) and the absorbance was measured at 510 nm. The output voltage V_d from the detector (1 V per absorbance unit) was quantized by an A/D−D/A converter (Measurement Computing, PC−CARD−DAS16/12−AO, USA) and acquired in a computer (PC; IBM ThinkPad 1843-BLJ, USA) as a Microsoft Excel format. An in-house program written in Excel VBA was used to acquire data, analyze them, and graphically display the results automatically. The FFT algorithm was referred to a book authored by Nakamura [37].

3.4. Software parameters

Table 1 lists the parameters for the flow rate modulation, data acquisition, and FFT. Control voltages, V_{c1} and V_{c2}, were varied in the -5 − +5 V and 0 − +2.5 V ranges with the 60 s and 30 s periods, respectively. Therefore, T in Eqs. (1)–(11) is 60 s and this period is automatically set as the time length of the FFT window. V_{c1}, V_{c2}, and V_d are acquired at the sampling frequency of 2.1333 Hz (every 0.46875 s). V_d is recorded after multiplying by 10 for easy comparison with V_{c1} and V_{c2}. Thus, 128 data are, respectively, obtained in the period of 60 s. Being considered the computer's processing speed, sixteen (= 2^4) data in T (i.e., every eighth 16 points) are used for FFT. The FFT computation is carried out every 3.75 s by using a new set of 16 data.

4. Results and discussion

In order to validate Eq. (14), 0 – 0.20 mmol dm^{-3} Fe^{3+} (the species B) solutions that did not contain Fe^{2+} (the species A) were analyzed with

Table 1
Analytical parameters.

Main parameters		Values
Modulation		
V_{c1}	Amplitude / V	5
	Offset voltage / V	0
	Period / s	60
V_{c2}	Amplitude / V	1.25
	Offset voltage / V	1.25
	Period / s	30
Data acquisition and analysis		
Sampling frequency / Hz		2.13333 (2)
Amplification factor for V_d		10
Number of data for FFT analysis		16
Interval of FFT analysis / s		3.75 (4)

The values in the parentheses are original values inputted by an operator. Sampling frequency and interval of FFT analysis are automatically changed to the higher and shorter values than the inputted values, respectively, so that they are compatible with the butterfly computation algorithm in FFT.

Table 2
The relationship between the amplitudes of the fundamental wave component and the second harmonic wave component due to Fe^{3+}.

C_B / mmol dm^{-3}	$A_{1,B}$ / V	$A_{2,B}$ / V	$A_{2,B}/A_{1,B}$
0	0.0100 ± 0.0007	0.0109 ± 0.0005	–
0.05	0.2739 ± 0.0030	0.1615 ± 0.0015	0.5897
0.1	0.5342 ± 0.0012	0.3178 ± 0.0021	0.5949
0.15	0.7980 ± 0.0023	0.4688 ± 0.0012	0.5875
0.2	0.9851 ± 0.0023	0.5788 ± 0.0023	0.5875

Amplitudes are expressed as mean ± s.d. (n = 23). The symbols B in the subscripts corresponds to Fe^{3+} in this experiment. Amplitudes of 1 V correspond to an absorbance of 0.1.

the present system. The amplitude of the second harmonic wave component (A_2) is considered the same as $A_{2,B}$ in the absence of Fe^{2+} (see Eq. (16)). Table 2 lists the results for $A_{1,B}$, $A_{2,B}$ and $A_{2,B}/A_{1,B}$. Theoretically, $A_{1,B}$ and $A_{2,B}$ should be zero at C_B is zero. The slight values (0.0100 and 0.0109 V, respectively) are considered to be experimental errors. The ratios of $A_{2,B}/A_{1,B}$ were found to be 0.5897, 0.5949, 0.5875 and 0.5875 at the Fe^{3+}concentrations (C_B) of 0.05, 0.10, 0.15, 0.20 mmol dm^{-3}, respectively. These values agreed fairly well with the theoretical value of $3\pi/16$ (~ 0.5890) in Eq. (14). Hereafter, Eq. (17) using the mean of the experimental values, 0.5899, was used for data analyses instead of Eq. (16).

$$A_2 = A_{2,A} + 0.5899A_1 \tag{17}$$

Fig. 3A shows an example of the control signals (V_{c1} and V_{c2}) and the analytical signal (V_d), where the concentrations of Fe^{2+} and Fe^{3+} in the sample were 0.1 and 0.2 mmol dm^{-3}, respectively. Analytical signals are moving averaged values, each using 3 data points. The t_{lag} estimated from the V_d's phase delay from the control signal's phase was 19.6 s. Fig. 3B shows the amplitudes of wave components obtained by FFT. FFT computation started at 67.03 s because V_d data at least in one FFT window (60 s) needs to be accumulated for the computation. Because 16 data were used for the FFT computation, up to the eighth harmonic wave component could be obtained based on the Nyquist sampling theorem [38]. The direct current component value and the third and fourth harmonic wave components' amplitudes were also plotted as references. The fundamental and the second harmonic wave components' amplitudes were 0.5405 ± 0.0048 V and 1.1559 ± 0.0050 V, respectively (n = 23). The respective relative standard deviations of 0.891% and 0.435% indicate the present method's high precision.

Various concentrations (0 – 0.20 mmol dm^{-3}) of Fe^{2+} or Fe^{3+} were measured, respectively, in the presence of 0.1 mmol dm^{-3} of the other ion. Fig. 4A and B shows the respective V_d measured, where the signals
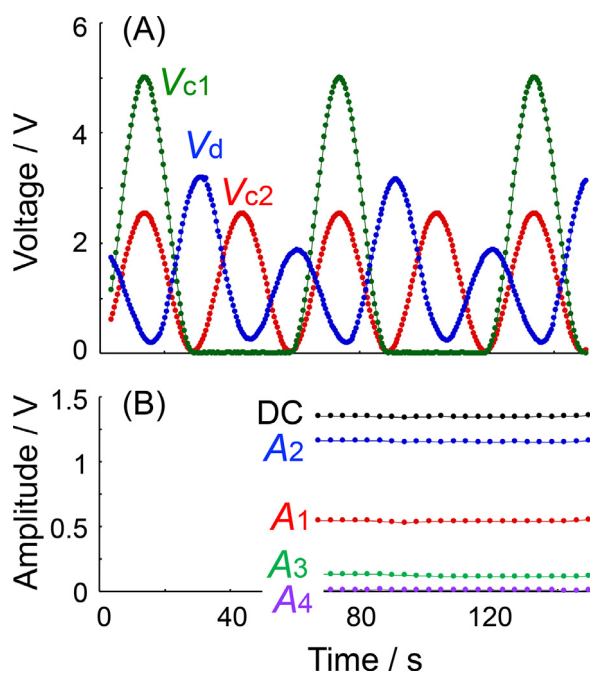
Fig. 3. (A) Example of control signals (V_{c1} and V_{c2}) and analytical signal (V_d). The concentrations of Fe^{2+} and Fe^{3+} in the sample were 0.1 and 0.2 mmol dm^{-3}, respectively. Analytical parameters were the same as those listed in Table 1. In our program, V_{c1} was recorded as 0 V when it was negative. (B) Amplitudes of wave components obtained by FFT analysis for V_d shown in Fig. 3A. DC, the direct current component; A_1, A_2, A_3, and A_4, the amplitudes of the fundamental, the second harmonic, the third harmonic, and the fourth harmonic wave components. Analytical signal and amplitudes of 1 V correspond to an absorbance of 0.1.
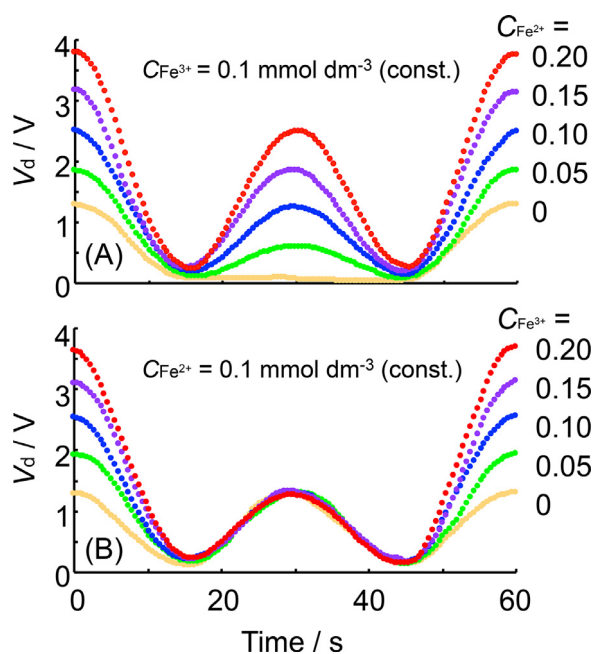

Fig. 4. Analytical signals for preparing calibration curves. (A) The concentration of Fe^{2+} was changed from 0 to 0.2 mmol dm^{-3} while that of Fe^{3+} was held constant at 0.1 mmol dm^{-3}. (B) The concentration of Fe^{3+} was changed from 0 to 0.2 mmol dm^{-3} while that of Fe^{2+} was held constant at 0.1 mmol dm^{-3}. The signals were superimposed so that they coincide in the phase. Analytical signals of 1 V correspond to an absorbance of 0.1.
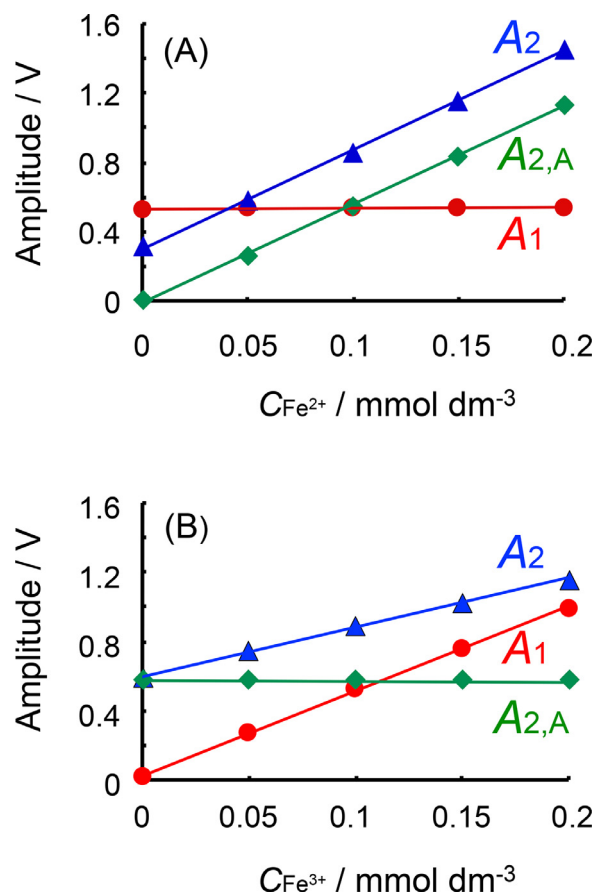

Fig. 5. Calibration curves for Fe^{2+} (A) and Fe^{3+} (B) in the presence of 0.1 mmol dm^{-3} of the other ion. The signals shown in Fig. 4 were used for preparing the calibration curves. Red circles: amplitude (A_1) of the fundamental wave component. Blue triangles: amplitude (A_2) of the second harmonic wave component. Green diamonds: net amplitude ($A_{2,Fe2+}$) of the second harmonic wave component caused by Fe^{2+}. Amplitudes of 1 V correspond to an absorbance of 0.1. (For interpretation of the references to color in this figure legend, the reader is referred to the web version of this article.)

were superimposed so that they coincided in the phase. The signals in the periods of 0–15 s and 45–60 s were obtained when L-ascorbic acid (AA) was delivered (positive V_{c1}); the signal in 15–45 s was obtained when AA was not fed (negative V_{c1}). In the latter period, only Fe^{2+} reacted with o-Phen. Therefore, V_d in Fig. 4A is increased with C_{Fe2+}, whereas V_d in Fig. 4B is constant irrespective of C_{Fe3+}, in this period. Fig. 5A and B shows the calibration curves for Fe^{2+} and Fe^{3+}, respectively, constructed from the data shown in Fig. 4A and B. The error of each data, expressed as a standard deviation (s.d.), is so small that the error bar is hidden in each data plot. Therefore, the numerical values for Fig. 5A and B, including s.d., are listed in Table S1A and B, respectively, in the Supplementary Material. In Fig. 5A, A_1 (plots in red circles) was almost constant at 0.5325 ± 0.0007 V because only Fe^{3+} (constant at 0.1 mmol dm^{-3}) contributed to A_1 (Eq. (15)). On the other hand, A_2 (plots in blue triangles) linearly increased with the Fe^{2+} concentration ($A_2/V = 5.7057C_{Fe2+}/(mmol\ dm^{-3}) + 0.3004$, $r^2 = 0.9993$). Net amplitude for $Fe^{2+}(A_{2,A})$ can be estimated from A_2 by considering the contribution of Fe^{3+} to A_2, according to Eq. (17). The obtained $A_{2,A}$ (plots in green diamonds) is in proportion to C_{Fe2+} with the intercept of nearly zero ($A_{2,A}/V = 5.6669C_{Fe2+}/(mmol\ dm^{-3}) - 0.0098$, $r^2 = 0.9991$). The limit of detection (3.3σ) for Fe^{2+} was 0.0071 mmol dm^{-3}.

Similarly, A_1 (in red circles), A_2 (in blue triangles) and $A_{2,A}$ (in green diamonds) are plotted as a function of the Fe^{3+} concentration in Fig. 5B. It shows A_1 and A_2 are increased in proportion to C_{Fe3+} ($A_1/V = 4.8721C_{Fe3+}/(mmol\ dm^{-3}) + 0.0246$, $r^2 = 0.9993$;

Table 3
Recovery test for real water samples.

Sample	$C_{Fe2+,add}$ / mmol dm^{-3}	$C_{Fe3+,add}$ / mmol dm^{-3}	$C_{Fe2+,found}$ / mmol dm^{-3}	$C_{Fe3+,found}$ / mmol dm^{-3}	Recovery of Fe^{2+}, %	Recovery of Fe^{3+}, %
Yoshino River	0	0	N.D.	N.D.	–	–
	0.1	0	0.099 ± 0.000	N.D.	99.4 ± 0.2	–
	0	0.1	N.D.	0.098 ± 0.002	–	98.6 ± 2.4
	0.1	0.1	0.098 ± 0.003	0.102 ± 0.002	98.6 ± 3.3	102.4 ± 1.4
Sako River	0	0	N.D.	N.D.	–	–
	0.1	0	0.102 ± 0.000	N.D.	102.4 ± 0.2	–
	0	0.1	N.D.	0.100 ± 0.002	–	99.8 ± 2.1
	0.1	0.1	0.102 ± 0.002	0.097 ± 0.001	102.5 ± 2.7	97.5 ± 1.0
Fuigo-onsen Spring	0	0	N.D.	N.D.	–	–
	0.1	0	0.102 ± 0.001	N.D.	102.1 ± 1.4	–
	0	0.1	N.D.	0.099 ± 0.001	–	99.1 ± 1.6
	0.1	0.1	0.103 ± 0.001	0.099 ± 0.002	103.0 ± 0.9	99.0 ± 1.7

($n = 3$)

Concentrations of ferrous and total iron in the Fuigo-onsen Spring water determined by a batch method (Japanese Industrial Standard (JIS) K0102) were 0.0018 mmol dm^{-3} and 0.0025 mmol dm^{-3}, respectively. The concentrations in other samples were below LOD (0.0006 mmol dm^{-3}).

$A_2/V = 2.8593C_{Fe3+}/$(mmol dm^{-3}) + 0.5928, $r^2 = 0.9991$). The ratio of the slopes of A_2 to A_1 (2.8593/4.8721 = 0.5869) is agreed with the theoretical value ($3\pi/16$ (~ 0.5890)) with the relative error of 0.36%. As expected, $A_{2,A}$ obtained from A_1 and A_2 by using Eq. (17) is constant at 0.5768 ± 0.0022 V regardless C_{Fe3+}, because C_{Fe2+} was invariable at 0.1 mmol dm^{-3}. The limit of detection (3.3σ) for Fe^{3+} was 0.0062 mmol dm^{-3}.

In the present system, 16 (= 2^4) data points were used for the real-time FFT computation, as described in Section 3.3. It is interesting to investigate whether a better LOD can be obtained if more data points are used on a computer with a higher speed. Therefore, all 128 (= 2^7) data points in an FFT window of 60 s (0.93750 – 60.93750 s) were analyzed after the measurement. The results are shown in Fig. S1 and Table S2 in the Supplementary Material. The LODs using 128 data points (0.0065 and 0.0054 mmol dm^{-3} for Fe^{2+} and Fe^{3+}, respectively) were only slightly better than those with 16 data points (0.0071 and 0.0062, respectively). It can be said, therefore, that 16 data points are acceptable enough to obtain good FFT results.

The theory was further validated by a recovery test using the real water samples. A 0.1 mmol dm^{-3} Fe^{2+} and/or the same concentration of Fe^{3+} were/was spiked in each sample and analyzed with the present system. Table 3 lists the results. Good recoveries around 100% (97.5% – 103.0%) were obtained for all the samples tested. The present system employed a common colorimetry (*o*-Phen spectrophotometry) with no preconcentration process. Therefore, there is room for further improvement in sensitivity for real sample analysis. However, the present results strongly support the validity of the proposed concept.

5. Conclusion

A concept of flow analysis for speciation is proposed. It is based on the modulation of flow rates of sample and redox pretreatment reagent solutions and the FFT analysis of analytical signal. The principle is described in detail. As proof of the concept, the speciation of Fe^{2+} and Fe^{3+} by *o*-Phen spectrophotometry was successfully carried out. The present amplitude modulated flow analysis can realize speciation from a single continuous analytical signal with a relatively simple flow system. A far as we know, the concept proposed in this study is a novel approach that has never been reported before.

On the principle of the discrete Fourier transform, the sample composition should be invariable within the FFT window range. This time length limits the sample throughput rate. In the present study for the proof of concept, 60 s was selected as the FFT window. This window could be shortened to about 10 s (*i.e.*, the V_{c1} and V_{c2} periods of 10 s and 5 s, respectively) at the expense of some precision [2].

The present approach has a potential feature of less susceptibility to baseline drift because the quantification is based not on the absorbance itself but the amplitude of the absorbance [3]; the drift does not affect the amplitudes of the fundamental and higher harmonic wave components, only the direct current value. This nature would be advantageous when colored species are liable to be absorbed on the optical cell window.

References

[1] H. Tanaka, T. Mima, M. Takeuchi, H. Iida, Amplitude modulated multiplexed flow analysis, Talanta 77 (2008) 576–580, doi:10.1016/j.talanta.2008.03.016.

[2] Y. Kurokawa, M. Takeuchi, H. Tanaka, Analytical parameters for amplitude modulated multiplexed flow analysis, Anal. Sci. 26 (2010) 791–796, doi:10.2116/analsci.26.791.

[3] T. Uemura, T. Ogusu, M. Takeuchi, H. Tanaka, Spectrophotometric determination of trace phosphate ion by amplitude-modulated flow analysis coupled with a malachite green method, Anal. Sci. 26 (2010) 797–801, doi:10.2116/analsci.26.797.

[4] K. Inui, T. Uemura, T. Ogusu, M. Takeuchi, H. Tanaka, Air-segmented amplitude-modulated multiplexed flow analysis, Anal. Sci. 27 (2011) 305–308, doi:10.2116/analsci.27.305.

[5] T. Ogusu, K. Uchimoto, M. Takeuchi, H. Tanaka, Air segmented-amplitude modulated multiplexed flow analysis with software-based phase recognition. Determination of phosphate ion, Talanta 118 (2014) 123–128, doi:10.1016/j.talanta.2013.10.001.

[6] K. Inui, H. Yoshida, M. Takeuchi, H. Tanaka, Application of air segmented amplitude modulated multiplexed flow analysis with software-based phase recognition to the determination of ammonium ion in water samples, J. Flow Inject. Anal. 32 (2015) 5–8, doi:10.24688/jfia.32.1_5.

[7] T. Sumiomo, M. Osaki, T. Ogusu, M. Takeuchi, H. Tanaka, Internal standard–amplitude modulated multiplexed flow analysis, Anal. Sci. 33 (2017) 1363–1368, doi:10.2116/analsci.33.1363.

[8] H. Yoshida, K. Inui, M. Takeuchi, H. Tanaka, Simultaneous determination of nitrite and nitrate ions by air-segmented amplitude modulated multiplexed flow analysis, Anal. Sci. 28 (2012) 523–525, doi:10.2116/analsci.28.523.

[9] L. Ma, M. Oshima, S. Motomizu, T. Hattori, Simultaneous determination of nitrate and nitrite ion by micro-flow injection analysis, Bunseki Kagaku 47 (1998) 375–380, doi:10.2116/bunsekikagaku.47.375.

[10] M. Troyanowics, Flow Injection Analysis, World Scientific, Singapore, 2000 Chap. 7.

[11] F. Zheng, S. Quian, S. Li, X. Huang, L. Lin, Speciation of antimony by preconcentration of Sb(III) and Sb(V) in water samples onto nanometer-size titanium dioxide and selective determination by flow injection-hydride generation-atomic absorption spectrometry, Anal. Sci. 22 (2006) 1319–1322, doi:10.2116/analsci.22.1319.

[12] D.G. Themelis, F.S. Kita, A. Economou, Flow Injection direct spectrometric assay for the speciation of trace chromium(III) and chromium(VI) using chromotropic acid as chromogenic reagent, Talanta 69 (2006) 615–620, doi:10.1016/j.talanta.2005.10.031.

[13] C. Lee, B. Chen, Y. Huang, Determining Cr(III) and Cr(VI) in urine using a flow injection on-line sorption separation system coupled with electrothermal atomic absorption spectrometry and a UV/nano-Au/TiO$_2$ photocatalysts reduction device, Talanta 77 (2008) 546–550, doi:10.1016/j.talanta.2008.03.018.

[14] S. Ohira, K. Nakamura, M. Chiba, P.K. Dasgupta, K. Toda, Matrix isolation with an ion transfer device for interference-free simultaneous spectrophotometric determinations of hexavalent and trivalent chromium in a flow-base system, Talanta 164 (2017) 445–450, doi:10.1016/j.talanta.2016.08.079.

[15] M. Noroozifar, M. Khorasani-Motlagh, A. Taheri, M. Homayoonfard, Application of manganese(IV) dioxide microcolumn for determination and speciation of nitrite and nitrate using a flow injection analysis-flame atomic absorption spectrometry system, Talanta 71 (2007) 359–364, doi:10.1016/j.talanta.2006.04.009.

[16] J. Wei, N. Teshima, T. Sakai, Flow injection analysis for oxidation state speciation of vanadium(IV) and vanadium(V) in natural water, Anal. Sci. 24 (2008) 371–376, doi:10.2116/analsci.24.371.

[17] M.K. Sengupta, P.K. Dasgupta, Oxidation state-differentiated measurement of aqueous inorganic arsenic by continuous flow electrochemical arsine generation coupled to gas-phase chemiluminescence detection, Anal. Chem. 83 (2011) 9378–9383, doi:10.1021/ac201972m.

[18] B. Haghighi, A. Safavi, Simultaneous flow injection determination of iron(II) and iron(III) with opto-electrochemical detection, Anal. Chim. Acta 354 (1997) 43–50, doi:10.1016/S0003-2670(97)00436-4.

[19] N. Youngvises, K. Suwannasaroj, J. Jakmunee, A. AlSuhaimi, Multi-reverse flow injection analysis integrated with multi-optical sensor for simultaneous determination of Mn(II), Fe(II), Cu(II) and Fe(III) in natural waters, Talanta 166 (2017) 369–374, doi:10.1016/j.talanta.2016.01.052.

[20] M. Novoč, M. Novič, J. Zupan, N. Zafran, B. Pihlar, Simultaneous determination of iron(II) and iron(III) by flow injection analysis. A mathematical simulation of the detector response, Anal. Chim. Acta 348 (1997) 101–111, doi:10.1016/S0003-2670(97)00096-2.

[21] A.F. Oliveira, J.A. Nóbrega, O. Fatibello-Filho, Asynchronous merging zones system: spectrophotometric determination of Fe(II) and Fe(III) in pharmaceutical products, Talanta 49 (1999) 505–510, doi:10.1016/S0039-9140(99)00015-6.

[22] K. Saitoh, T. Hasebe, N. Teshima, M. Kurihara, T. Kawashima, Simultaneous flow-injection determination of iron(II) and total iron by micelle enhanced luminol chemiluminescence, Anal. Chim. Acta 376 (1998) 247–254, doi:10.1016/S0003-2670(98)00539-X.

[23] D.G. Themelis, P.D. Tzanavaras, F.S. Kika, M.C. Sofoniou, Flow-injection manifold for the simultaneous spectrophotometric determination of Fe(II) and Fe(III) using 2,2'-dipyridyl-2-pyridylhydrazone and a single-line double injection approach, Fresenius J. Anal. Chem. 371 (2001) 364–368, doi:10.1007/s002160100930.

[24] R. Kuroda, T. Nara, K. Oguma, Simultaneous determination of iron(III) and total iron by flow injection analysis using kinetic spectrophotometry with Tiron, Analyst 113 (1988) 1557–1560, doi:10.1039/AN9881301557.

[25] M. Kass, A. Ivaska, Spectrophtometric determination of iron(III) and total iron by sequential injection analysis technique, Talanta 58 (2002) 1131–1137, doi:10.1016/S0039-9140(02)00439-3.

[26] L.V. Mulaudzi, J.F. van Staden, R.I. Stefan, On-line determination of iron(II) and iron(III) using a spectrophotometric sequential injection system, Anal. Chim. Acta 467 (2002) 35–49, doi:10.1016/S0003-2670(02)00128-9.

[27] C. Pons, R. Forteza, V. Cerdà, Multi-pumping flow system for the determination, solid-phase extraction and speciation analysis of iron, Anal. Chim. Acta 550 (2005) 33–39, doi:10.1016/j.aca.2005.06.072.

[28] J. Paluch, J. Kozak, M. Wieczorek, M. Kozak, J. Kochana, K. Widurek, M. Konieczna, P. Kościelniak, Novel approach to two-componet speciation analysis. Spectrophotometric flow-based determination of Fe(II)/Fe(III) and Cr(III)/Cr(VI), Talanta 171 (2017) 275–282, doi:10.1016/j.talanta.2017.05.005.

[29] A. Saavedra, E. Donati, E. Cortón, Reagent-free flow-injection amperometric sensor for quantification and speciation of iron for bio-hydrometallurgical applications, Sens. Actuator B 220 (2015) 448 -445, doi:10.1016/j.snb.2015.05.101.

[30] J. Kozak, J. Gutowski, M. Kozak, M. Wieczorek, P. Kościelniak, New method for simultaneous determination of Fe(II) and Fe(III) in water using flow injection technique, Anal. Chim. Acta 668 (2010) 8–12, doi:10.1016/j.aca.2010.02.002.

[31] J. Kozak, N. Jodłowska, M. Kozak, P. Kościelniak, Simple flow injection method for simultaneous spectrophotometric determination of Fe(II) and Fe(III), Anal. Chim. Acta 702 (2011) 213–217, doi:10.1016/j.aca.2011.06.053.

[32] J. Kozak, J. Paluch, A. Węgrzecka, M. Kozak, M. Wieczorek, J. Kochana, P. Kościelniak, Single peak parameters technique for simultaneous measurements: spectrophotometric sequential injection determination of Fe(II) and Fe(III), Talanta 148 (2016) 626–632, doi:10.1016/j.talanta.2015.06.040.

[33] R.B.R. Mesquita, R. Suárez, V. Cerda, M. Rangel, A.O.S.S. Rangel, Exploiting the use of 3,4-HPO ligands as nontoxic reagents for the determination of iron in natural waters with a sequential injection approach, Talanta 108 (2013) 38–45, doi:10.1016/j.talanta.2013.02.058.

[34] J.L.A. Miranda, R.B.R. Mesquita, A. Nunes, M. Rangel, A.O.S.S. Rangel, Iron speciation in natural waters by sequential injection analysis with a hexadentate 3-hydroxy-4-pyridinone chelator as chromogenic agent, Talanta 148 (2016) 633–640, doi:10.1016/j.talanta.2015.05.062.

[35] J.T. Dyke, Q.T. Fernando, Deconvolution techniques for rapid flow-injection analysis, Talanta 32 (1985) 807–810, doi:10.1016/0039-9140(85)80187-9.

[36] B. Szostek, M. Trojanowicz, Flow-injection analysis using Fourier transform of a multiple injection signal, Chemom. Intell. Lab. Syst. 22 (1994) 221–228, doi:10.1016/0169-7439(93)E0051-5.

[37] S. Nakamura, Beginner's Digital Fourier Transform, Tokyo Denki University Press, Tokyo, 1989.

[38] D.A. Skoog, F.J. Holler, S.R. Crouch, in: Principles of Instrumental Analysis, 7th ed., Cengage Learning, Boston, 2018, pp. 105–106.